Springer

Journal of
Mechanical
Science and
Technology

Journal of Mechanical Science and Technology 23 (2009) 874~884

www.springerlink.com/content/1738-494x
DOI 10.1007/s12206-009-0104-2

A study on the slip velocity on a pair of asymmetric electrodes for AC-electroosmosis in a microchannel †

Yangyang Wang, Yong Kweon Suh and Sangmo Kang*

Department of Mechanical Engineering, Dong-A University, Busan, 604-714, Korea

(Manuscript Received November 11, 2008; Revised December 1, 2008; Accepted January 8, 2009)

Abstract

In numerical studies on microscale electroosmotic flows, the electric double layer (EDL) effect is usually predicted by solving the traditional Navier-Stokes equation subjected to the slip velocity induced by the electric-charged wall as a boundary condition. Recently, Suh and Kang (Physical Review E **77**, 2008) presented the asymptotic solutions of the ion transport equations near a polarized electrode under the action of an AC field, and then proposed a new theoretical model of the slip velocity on the electrode considering the ion adsorption effect. In the present paper, we apply the model to a two-dimensional AC-electroosmotic flow in a microchannel to calculate the slip velocity on a pair of coplanar asymmetric electrodes embedded on the bottom wall, and then experimentally measure the slip velocity using the micro-PIV technique to validate the theoretical model. Comparison shows an excellent overall match between the theoretical and experimental results, except for on the narrow electrode at low frequencies. Next, we numerically perform parametric studies regarding the AC frequency, effective Stern-layer thickness and ion adsorption effect to further understand the characteristics of the AC electroosmotic flow. Results show that, as the frequency increases, the slip velocity also increases. In addition, the velocity decreases with increasing either Stern-layer thickness or ion adsorption effect.

Keywords: AC-electroosmosis; Effective Stern-layer thickness; Ion adsorption; Slip velocity; Particle image velocimetry (PIV)

1. Introduction

A charged solid wall when brought in contact with an electrolyte containing free ions attracts the counterions dissolved in the electrolyte and repels the coions, resulting in the unbalanced distribution of ions in the very thin layer immediately next to the surface. Such a layer is called the electric double layer (EDL) and the net charge in the layer has to electrically counterbalance the surface charge. Note that most dielectric substances become naturally charged, mainly with a negative sign due to the ionization of a surface group or ion absorption, when in contact with an aqueous solution. In addition, the surface charge can also be obtained artificially by embedding an electrode on the surface and supplying a direct-current (DC) potential on it. If the electric field is externally applied tangentially to the surface, all the fluid out of the layer as well as in the layer is forced to flow along the surface because of the electro-migration of ions and the fluid viscosity. Such an electrokinetic flow is called the DC-electroosmotic flow (DCEF) and can be very usefully exploited to pump and mix fluids in microscale channels (see Li [1] for a more detailed review).

If an alternating-current (AC) potential is imposed on the electrodes (usually in pairs), on the other hand, another kind of flow pattern is observed. Two coplanar electrodes which are embedded with a small gap on a wall surface immersed in an electrolyte solution generate a new unsteady distribution of ions in the

† This paper was recommended for publication in revised form by Associate Editor Dongshin Shin

* Corresponding author. Tel.: +82 51 200 7636, Fax.: +82 51 200 7656
E-mail address: kangsm@dau.ac.kr

© KSME & Springer 2009

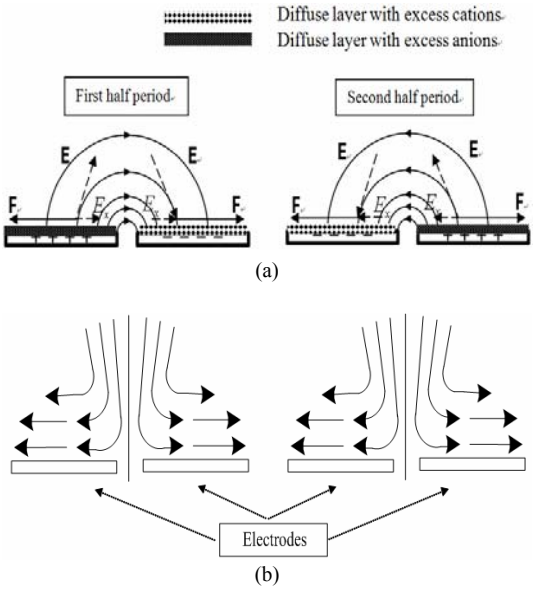

Fig. 1. A schematic diagram describing the mechanism of the AC-electroosmotic flow (ACEF): (a) electric field and (b) fluid flow.

solution when the AC potential is applied with opposite signs on the electrodes, as shown in Fig. 1. In the first half-period when the left electrode is positively charged and the right one is negatively, the excess anions are accumulated onto the left electrode and the excess cations are onto the right one, leading to the formation of a nonuniform unsteady electric field. On both electrodes, nonzero tangential components of the electric field (denoted by E_x in the figure) are produced and they all are directed from the left side to the right. Accordingly, the excess anions accumulated on the left electrode are forced to move toward the left side, whereas the excess cations on the right electrode are to move toward the right side. In other words, the fluid surrounding them near the electrodes is also driven to flow from the center of the gap to both outer edges of the electrodes, giving rise to the secondary flow pulled down toward the surface to fill the depleted region around the gap center. In the second half-period where the sign of the AC potential is reversed, on the contrary, the direction of the electric field and the signs of the excess ions on both electrodes are simultaneously reversed, indicating that the direction of the induced secondary flow stays unchanged. After all, a steady flow is generated even under the action of the AC potentials on the coplanar electrodes, mainly at moderate to high frequencies, and is called the AC-electroosmotic flow (ACEF) [2].

Because of such steady flow characteristics, ACEF can also be applied to pump and mix fluids in microscale channels [3-9]. Recently, increasingly more attention has been paid to ACEF because of its many advantages compared with DCEF. It requires so small voltage (less than 5V) that the electrode degradation can be reduced and the air-bubble generation can be prevented. In addition, the fluid properties are not significantly changed and the energy consumption is very low.

The Poisson-Nernst-Planck (PNP) model and Poisson-Boltzmann (PB) model have been successfully applied to the numerical simulations of electroosmotic flows in microscales [1, 10-12]. In addition to the momentum equations containing the electric force term for the flow field, the PNP model requires solving the Nernst-Planck equation and Poisson equation for the ionic distribution and electric potential, respectively, whereas the PB model needs to apply the Boltzmann-distribution assumption for the ionic distribution and solve the Poisson equation for the electric potential. In addition, another kind of numerical model, usually called the slip-velocity model, has been also applied to the numerical simulations because it can significantly reduce the computational effort compared to PNP and PB models [13-15]. In microscale electroosmotic flows, most of the excess charges are clustered in the EDL adjacent to the wall surface whose thickness is very small compared with the channel dimension. That is, the electric force is exerted only in this layer and thus the fluid is driven to move there. Then, the fluid in the bulk is forced to also move by the fluid motion in the EDL due to the fluid viscosity. If the velocity in the EDL is known in advance, therefore, the momentum equation without the electric force term (i.e., Navier-Stokes equation) can be directly solved for the flow field in the bulk region. In such a case, the electric effect has to be replaced with the tangential velocity at the solid wall, usually called the slip velocity, as a boundary condition. In the DC case, the slip velocity, u_{slip}, can be obtained relatively easily by using the well-known Helmholtz-Smoluchowski equation [16]:

$$u_{slip} = \frac{\varepsilon\varepsilon_0\zeta}{\eta}\frac{\partial\phi}{\partial x_s}, \tag{1}$$

where ε is the relative permittivity (dimensionless) of the fluid, ε_0 the dielectric permittivity of the vacuum, η the fluid viscosity, ζ the zeta potential,

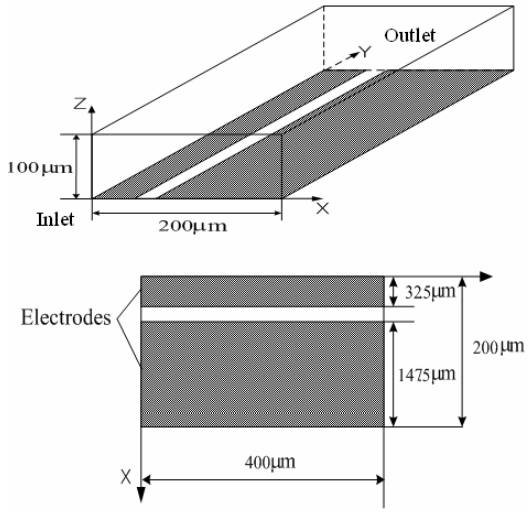

Fig. 2. Schematic diagrams of the flow geometry and electrode array.

ϕ the external electric potential, and x_s the wall-tangential coordinate. The external potential ϕ is almost undisturbed by the existence of EDL because either the wall is parallel to the electric field $\nabla\phi$ or the zeta potential remains small in magnitude. In the AC case, however, the slip velocity cannot be obtained so easily, mainly because the external potential is significantly disturbed by the EDL and it is to be determined from the interaction between the bulk and the EDL in terms of the ion transport. For the efficient application of the model, therefore, accurate information of the slip velocity on the electrodes is indispensable.

So far, some researches have been numerically and experimentally performed on the slip veocity on the electrodes under the action of AC [2, 17-19]. González et al. [17] derived the slip velocity on the microelectrodes subjected to the AC potential, using a simple capacitor model, under the assumption that the double-layer thickness is much smaller than the electrode dimension and the linear approximation applies. Subsequently, Green et al. [2] calculated the potential drop across the EDL at the surface of the electrodes using the linear EDL theory and also the impedance of the EDL obtained from the experimental data, and then predicted the AC slip velocity on the electrodes using the Helmholtz-Smoluchowski formula. Very recently, Suh and Kang [19] showed that the electric layer near an electrode surface under an AC electric field should be of a triple-layer structure: the Stern layer, inner layer and middle layer (or buffer layer). Then, they presented a new asymptotic model for computing the slip velocity by incorporating the effect of the ion adsorption onto the electrode. The model is composed mainly of solving the Laplace equation for the electric potential in the bulk region and a dynamic equation for the evolution of the surface charge on the electrode representing the ion transport within the layer. Despite much advancement of the slip-velocity model, the model was applied only to one-dimensional flow in the study.

In the present study, we numerically apply the theoretical model proposed by Suh and Kang [19] to the two-dimensional AC electroosmotic flow on a pair of coplanar asymmetric electrodes embedded on the bottom wall of a rectangular channel to calculate the slip-velocity distribution. To validate the model, we also measure the slip velocity using micro-PIV (particle image velocimetry) technique and compare the experimental results with the numerical ones. After that, we perform numerical parametric studies regarding the AC frequency, effective Stern-layer thickness and ion adsorption effect to further understand the characteristics of the AC electroosmotic flow. This would contribute to further understanding of the AC electroosmotic flows in microfluidic devices.

2. Numerical methods

2.1 Flow geometry

Fig. 2 shows details of the flow geometry and electrode array used in the present study. The fluid is pressure-driven to flow through a very long channel with a uniform rectangular cross section of 200μm×100μm (width and height) and a pair of coplanar electrodes embedded on the bottom wall. The electrode pair is composed of two electrodes separated by a small gap, 20 μm, with different widths, 32.5μm (narrow electrode) and 147.5μm (wide one), but the same length, 400μm. In other words, the electrode array occupies the whole bottom wall of the channel over the length 400μm. For the AC electroosmosis, the AC electric potential is imposed on both electrodes with opposite signs. Note that the length of the electrode pair is taken long enough so that the flow can be considered two-dimensional in the numerical simulation. For convenience, the Cartesian coordinate system, (X, Y, Z), is adopted with its origin at the outer edge of the narrow electrode on the inlet, as shown in Fig. 2. As a working reference fluid,

a sodium chloride solution (NaCl, 1mM) is used to analyze the slip velocity. The reason for applying a pressure gradient along the longitudinal direction is that by measuring the longitudinal velocity we can estimate the vertical coordinate of a fluid particle of interest for measuring the flow field on a horizontal plane; both flows are assumed to be decoupled [20].

2.2 Theoretical model and numerical methods for the slip velocity

To compute the slip velocity on the pair of electrodes under the action of AC external electric field, we employ the theoretical model proposed by Suh and Kang [19] in the present study, which can be described as follows:

(i) Get the distribution of the external electric potential, ϕ, over the whole bulk region by solving the following Laplace equation subjected to an appropriate boundary condition at the wall, ϕ_w (to be given later):

$$\nabla^2\phi = 0. \tag{2}$$

Then, get the normal component of the electric field at the wall, $(\partial\phi/\partial x_n)_w$ (x_n denotes a wall-normal coordinate), from the solution.

(ii) Update the dimensionless surface-charge density at the wall, q, as follows:

$$\frac{dq}{dt} = \frac{\sqrt{2}\omega\lambda_{dif}}{(1+\beta)\varsigma_T}\left(\frac{\partial\phi}{\partial x_n}\right)_w, \tag{3}$$

where t denotes the time, ω the angular frequency of the AC potential, λ_{dif} the diffusion length scale or the middle-layer thickness ($\lambda_{dif} = \sqrt{D/\omega}$ where D is the ionic diffusivity), and ς_T the thermal potential. In addition, β is a dimensionless parameter defined as

$$\beta = \frac{8\sqrt{2}\Gamma_{max}\alpha\sqrt{\gamma}\left(8+16\alpha c_0+\gamma q^2\right)}{\lambda_{dif}\sqrt{16+\gamma q^2}\left(4+8\alpha c_0+\alpha c_0\gamma q^2\right)}, \tag{4}$$

where Γ_{max} is the maximum available dimensionless surface concentration of both ions adsorbed at the interface, c_0 the bulk concentration of both ions, $\gamma = \left(\lambda_{dif}/\sqrt{2}\lambda_d\right)^2$ (usually very large; here, λ_d is the Debye screening length), and α the parameter to control the increase rate of ionic surface concentration adsorbed upon change of ion concentration at the interface (see Suh and Kang [19] for details).

(iii) Calculate the electric potential at the wall, ϕ_w, as follows:

$$\phi_w = V_{oo}\cos\omega t + \left(\frac{\gamma\varsigma_T\lambda_{Seff}}{\sqrt{2}\lambda_{dif}}\right)q - \Delta\phi_S - \Delta\phi_i, \tag{5}$$

$$\Delta\phi_S = -\left(\frac{\gamma\varsigma_T\lambda_{Seff}}{\sqrt{2}\lambda_{dif}}\right)q - \left(\frac{\lambda_{Seff}}{\varepsilon\varepsilon_0}\right)\sigma_a, \tag{6}$$

$$\Delta\phi_i = \varsigma_T \ln\left(\frac{\sqrt{16/\gamma+q^2}-q}{\sqrt{16/\gamma+q^2}+q}\right), \tag{7}$$

where $\Delta\phi_S$ and $\Delta\phi_i$ denote the potential drops over the Stern layer and inner layer, respectively, V_{00} the amplitude of the AC potential, and λ_{Seff} the effective Stern-layer thickness. In addition, σ_a denotes the dimensionless surface charge density caused by the ion adsorption at the interface, which can be directly calculated as follows:

$$\sigma_a = \frac{\Gamma_{max} z e\alpha c_0\gamma q\sqrt{16/\gamma+q^2}}{4+8\alpha c_0+\alpha c_0\gamma q^2}, \tag{8}$$

where z is the ionic valence and e the elementary electron charge.

(iv) Increase the time level and repeat (i)-(iii).

Based on the temporal evolution of the electric potential, the instantaneous slip velocity, u_w, on the electrode surface can be calculated as follows:

$$u_w = \frac{\varepsilon\varepsilon_0}{\eta}\Delta\phi_i\left(\frac{\partial\phi_w}{\partial x_s}\right), \tag{9}$$

where ϕ_w needed for $\partial\phi_w/\partial x_s$ comes from the solution of Eq. (2). Finally, the steady slip velocity is given by taking the temporal averaging of the instantaneous one (9) over one cycle of the AC excitation as follows:

$$u_{slip} = \frac{\varepsilon\varepsilon_0}{\eta}\left\langle\Delta\phi_i\frac{\partial\phi_w}{\partial x_s}\right\rangle, \tag{10}$$

where $\langle\ \rangle$ denotes the time average.

We obtain the steady slip velocity on the pair of electrodes by applying the theoretical model to a two-

(a)

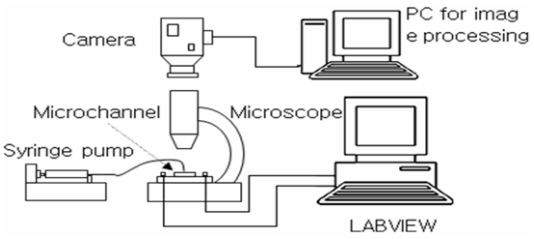

(b)

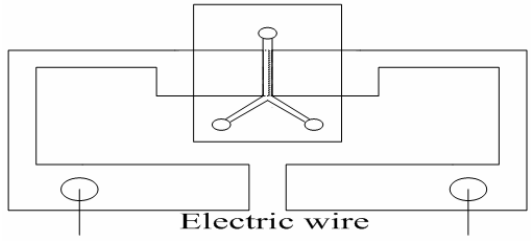

(c)

Fig. 3. Experiment setup: (a) real photo of the overall setup, (b) schematic diagram of the setup, and (c) schematic details of the test-section part.

dimensional cross section of the channel (on the XZ plane in Fig. 2) under the assumption that the channel is long enough. The SOR (successive over relaxation) method is used to solve the Laplace Eq. (2), while the Euler method is used to solve the time-evolution Eq. (3).

3. Experimental setup and methods

To validate the theoretical slip-velocity model, we perform experimental measurements using the micro-PIV system and then compare the numerical results with the experimental ones. The experimental setup used in the present study is shown in Fig. 3. For the experiment, LABVIEW is used to impose the AC potential on the microelectrodes and a CCD camera of 1360×1024 pixels and a microscope (BX51: Olympus) are used for observation and data-recording.

We use the PDMS channel, which is fabricated by pouring a mixture of Sylgard 184 silicon elastomer (DC-184A) and curing agent (DC-184B) (10:1) onto a mould, followed by curing it for 24 hours at 23°C. The cured PDMS is separated from the model. Then two holes are made at the end of the channel, using a 2-mm circular punching device, and are connected to the syringe pump and a waste box. Bonding of the PDMS and ITO glass substrate is made by using a high frequency generator (plasma generator, BD-10A). After the plasma-generator treatment, $-CH_3$ on the PDMS surface is replaced with H_2O and CO_2. As a result, Si-O-Si covalent bonding occurs between the glass substrate and PDMS [21]. Note that only the bottom surface made of ITO glass is to be considered. Although the zeta potential on the PDMS surface is known to evolve in time, it should not cause any experimental difficulty. The flow through the channel is pressure-driven by a syringe pump. As shown in Fig. 2, the configuration of the channel and electrode array is exactly the same as that used for the numerical simulation.

For the fluid, we use a sodium chloride solution (NaCl, 1mM) as a working reference fluid to analyze the slip velocity. In particular, the solution is chosen with the purpose of reducing the effect of ion concentration oscillation. The flow through the microchannel is observed by seeding particles. It is required that the particles should efficiently scatter light and be sufficiently small compared to the channel dimension. To avoid the Brownian motion, however, the particles should be bigger than 500nm [22, 23]. By selecting the particles with a nominal diameter of 1μm, we expect the effect of the Brownian motion to be substantially reduced [24]. At this time, the red fluorescent polymer micro spheres from Duke Scientific Corporation are used. The electrophoresis due to the particle can cause oscillation under an AC electric field. Only when the particles are attached onto the edge of the channel can a very weak oscillation be observed. Therefore, we can assume that the particle motion should be mostly ascribed to the fluid motion and the electrophoresis effect should be neglected. In other words, we expect that the particle motion should measure the real fluid motion.

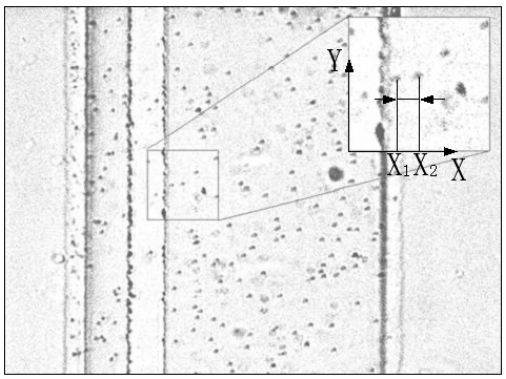

Fig. 4. One sample frame taken from the experiment, demonstrating how to measure the slip velocity.

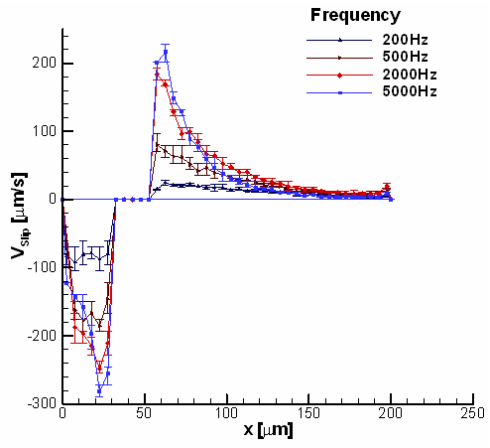

Fig. 5. Profiles of the slip velocity measured at different frequencies, ω = 200Hz, 500Hz, 2,000Hz and 5,000Hz.

4. Results and discussions

4.1 Experimental results

In the experiment, the average velocity is set as 50μm/s. At first, we bring the surface of the electrodes into focus. Then the 3V AC potential is applied onto the electrodes. To see the effect of the AC frequency on the slip velocity, experimental measurements are made for the frequencies ω = 100Hz, 200Hz, 300Hz, 500Hz, 1,000Hz, 2,000Hz, 3,000Hz and 5,000Hz. The camera speed is 20 frames per second and a total of 400 frames are taken for each frequency. In each frame, the particles attached onto the electrode surface can be recognized easily because the surface is a focus plan. From the movie frame, the positions and velocities of the particles (on the XY plane in Fig. 2) can be measured as follows. First, the positions of a particle, X_1 and X_2, are detected at two successive instants with a very short interval, t_0 and $t_0 + \Delta t$, as shown in Fig. 4. Then the slip velocity in the X-direction is calculated with $U = (X_2 - X_1)/\Delta t$ at a position, $X = (X_1 + X_2)/2$.

For more efficient data collection, the bottom area of the channel is divided into 41 grids. The velocity measured inside each grid is considered as the slip velocity at the center point of the grid. In the present study, four to ten velocity data are collected at each central point.

Fig. 5 shows profiles of the slip velocity experimentally measured at different frequencies: ω = 200 Hz, 500Hz, 2,000Hz and 5,000Hz. For all the frequencies, the slip velocity has the highest values at the two inner edges of the pair of electrodes and then decreases exponentially to a zero value with going towards the two outer edges. The slip velocity on the narrow electrode is higher than that on the wide electrode. In addition, as the frequency increases, the slip velocity also increases but the increase rate becomes lower. When the frequency is equal to 5,000Hz, the highest velocity on the narrow electrode approaches 280μm/s, while that on the wide electrode approaches 220μm/s.

4.2 Comparison between theoretical and experimental results

We perform numerical simulations on the XZ plane (see Fig. 2) to get the slip velocity on the pair of electrodes under an AC electric field by following the procedure explained in the subsection 2.1. Here, only the two-dimensional simulations are considered because the length of the channel (or the electrodes) is very large compared to the cross-section dimensions, and the main flow is too slow to affect the ACEO across the channel. Note that the model considered is exactly the same as the cross section of the channel used in the experiment. A grid system of 160×80 (on the XZ plane) is adopted to solve the Laplace equation (2) over the whole bulk region for the electric potential. As an example, the temporal evolution of the electric potential distribution computed at the frequency ω = 5,000Hz is shown in Fig. 6.

To validate the theoretical model, we compare the theoretical slip velocity with the experimental measurement. The comparison results are shown in Fig. 7 at different frequencies of the AC field. Note that λ_{Seff} = 40nm and $\alpha = 0.8\times10^{-26}$ are used for the numerical simulation and the details are explained in the

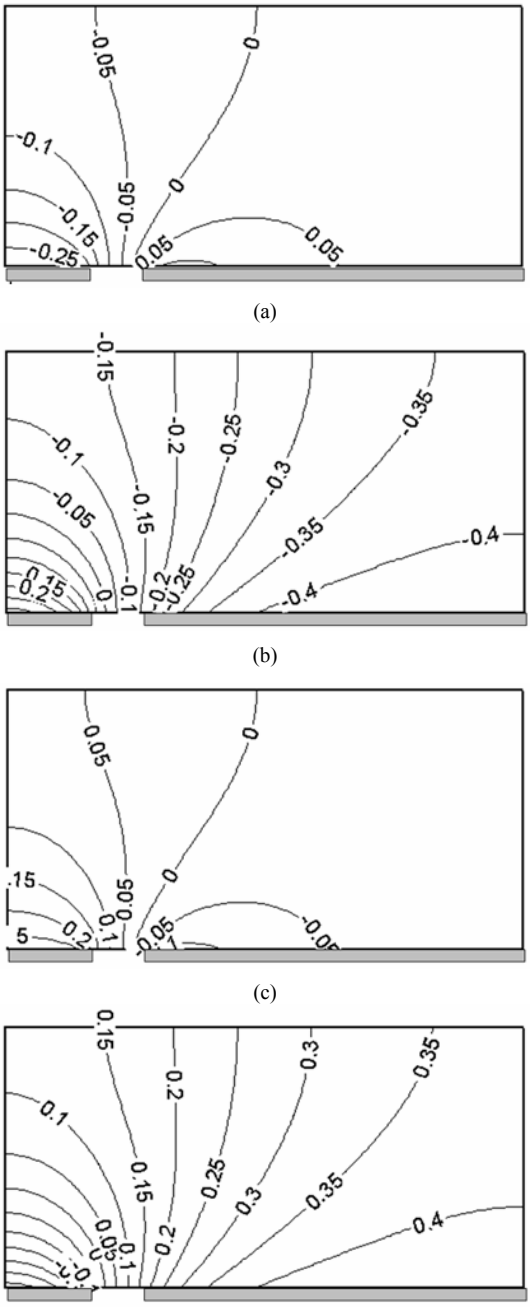

Fig. 6. Temporal evolution of the electric potential, ϕ [V], over a cross section of the channel for $\omega = 5{,}000$Hz: (a) t=0, (b) t=T/4, (c) t=T/2 and (d) t=3T/4 where T denotes the period of the AC excitation.

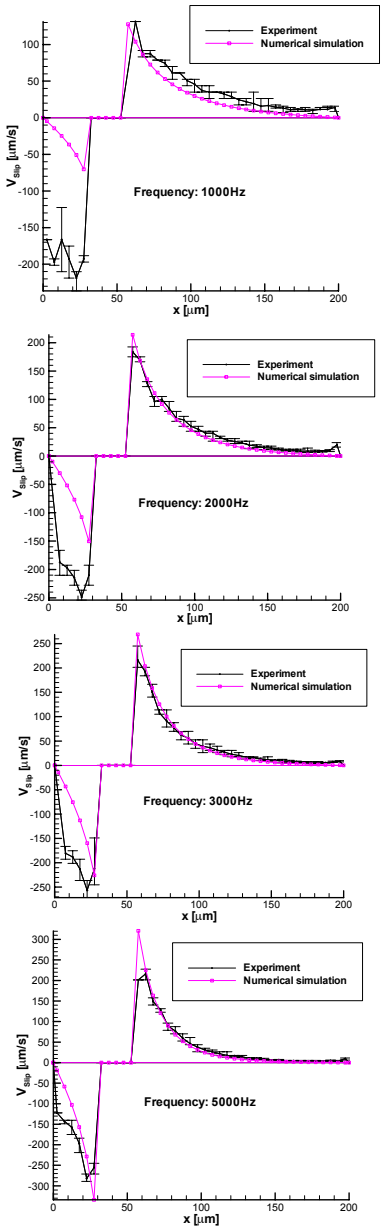

Fig. 7. Comparison of the slip velocity between the theoretical model and experiment measurement at different frequencies of the AC field: $\omega = 1{,}000$, 2,000, 3,000 and 5,000Hz. For the numerical simulations, $\lambda_{Seff} = 40$nm and $\alpha = 0.8 \times 10^{-26}$ are used.

next subsection. It is clearly seen that both profiles of the slip velocity on the wide electrode exhibit an excellent agreement at all the frequencies. On the narrow electrode, on the other hand, they show different degrees of match depending on the frequency. Very good match between both profiles is seen at a high frequency (for example $\omega = 5{,}000$Hz), whereas very poor match between them is seen at a low frequency. In other words, the discrepancy between them be-

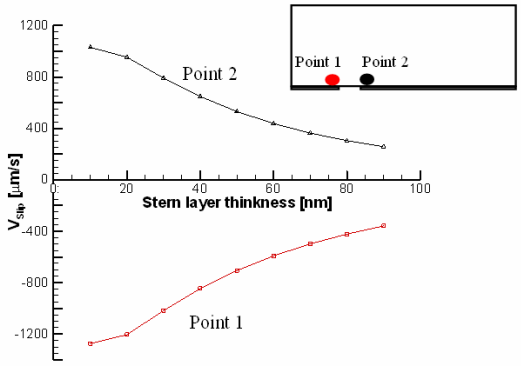

Fig. 8. Variations of the slip velocity with the effective Stern-layer thickness at two different points for ω = 5,000Hz.

comes more distinct and the error bar gets bigger with decreasing frequency. Although we guess that the difference may be caused by some unexpected background noise, the exact cause is not clear at the present instant and further study is necessary in the near future.

4.3 Parametric studies by the numerical simulateon

To see the effect of the electrode material on the slip velocity, detailed studies on the two more parameters have been performed: one is the effective Stern-layer thickness, λ_{Seff}, and the other is the parameter, α (see the previous subsection for the frequency). Note that the two parameters, λ_{Seff} and α, play critical roles in calculating the theoretical slip velocity.

The effect of the effective Stern-layer thickness on the slip velocity is illustrated in Fig. 8, which shows variations of the slip velocity with the layer thickness at two different points for the frequency $\omega = 5{,}000$Hz. Here, each of the two points is 5μm apart from the inner edge of its corresponding electrode. Clearly, as the layer thickness increases, the slip velocity markedly decreases. The flow characteristic is in exact agreement with that obtained for one-dimensional flow in Suh and Kang [19]. As the Stern-layer thickness increases, the potential drop across the inner layer, $\Delta\phi_i$, decreases and simultaneously the total potential drop across the Stern and inner layers, $\phi_0 - \phi_w = \Delta\phi_S + \Delta\phi_i$, increases, finally leading to the reduction of the potential at the outer edge of the diffuse layer, ϕ_w. Therefore, with increasing Stern-layer thickness, the slip velocity should decrease, as shown in Eq. (10).

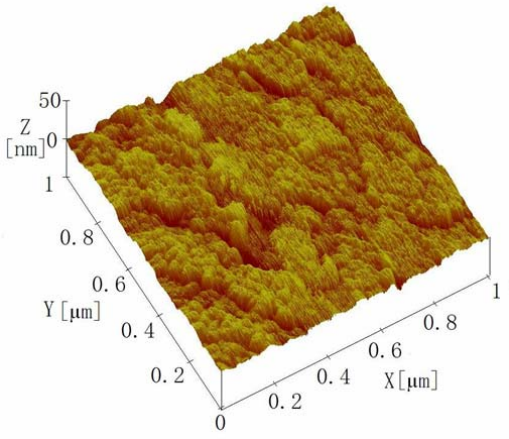

Fig. 9. 3D Atomic force microscope photo on the electrode surface where the overall size is 1 μm ×1μm (on the XY plane) and the Z direction is the roughness height.

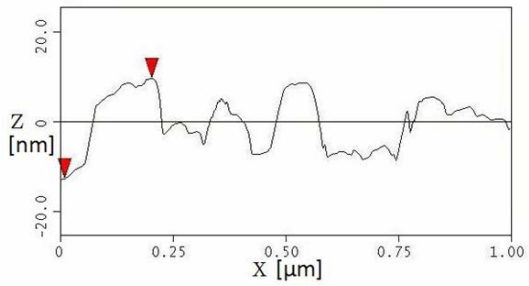

Fig. 10. Profile of the roughness on the electrode surface along a certain line in Fig. 9, where the triangles mark the highest and lowest points.

In the present numerical simulation, the effective Stern-layer thickness, λ_{Seff} = 40 nm, is chosen for the best match with the experimental result (see also subsection 4.2). Note that the layer thickness is usually about λ_{Seff} = 20nm [19]. To figure out the difference, we closely check the surface roughness on the ITO (Indium tin oxide) glass electrode used in the experimental measurement and present the results in Figs. 9 and 10. Fig. 9 shows the 3D AFM (atomic force microscope) photo on the surface of the electrode. It is evidently seen that the surface is not so smooth. To quantify the surface roughness, a profile of the roughness along a certain line is shown in Fig. 10. The profile indicates that the roughness size is approximately 20nm, which corresponds to the difference between the layer thickness chosen to match the experimental measurement (λ_{Seff} = 40nm) and the theoretical one (λ_{Seff} = 20nm). Therefore, it is estimated that the difference may come from the surface roughness of the

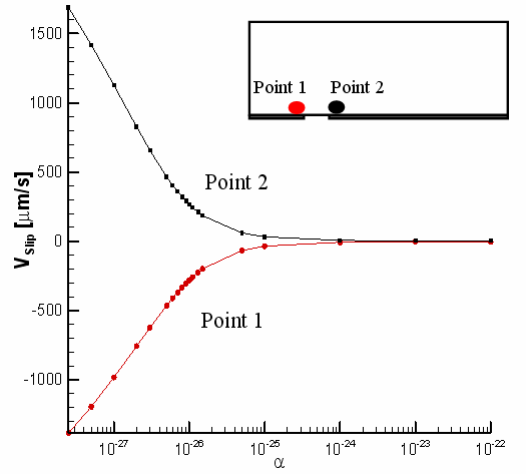

Fig. 11. Variations of the slip velocity with the parameter, α [m^3], at two different points for ω = 5,000Hz.

electrode. Note that the theoretical slip-velocity model derived in Suh and Kang [19] does not include the effect of surface roughness.

Then the effect of the parameter, α, on the slip velocity is also studied. Figure 11 shows variations of the slip velocity with the parameter at two different points for the frequency $\omega = 5{,}000$Hz. Here, the parameter, α, plays a role in controlling the rate of increase of ion surface concentration adsorbed at the interface upon change of ion concentration. In other words, as α increases, more counterions are absorbed at the interface between the Stern and inner layers, increasing the surface charge density. In such a case, there should be an increased jump in the potential gradient across the interface, finally decreasing the potential drop across the inner layer and thus the slip velocity [19]. The result is obviously illustrated in Fig. 11: as α increases, the slip velocity decreases. For the best match with the experimental result, $\alpha = 0.8\times10^{-26}$ is chosen in the numerical simulation.

5. Conclusion

The numerical simulation of electroosmotic flows usually requires the use of the Poisson-Nernst-Planck (PNP) model and Poisson-Boltzmann (PB) model. Since these models are very expensive, especially for the AC case, however, one useful substitute for them may be the so-called slip-velocity model. In the model, the flow is predicted by simply solving the traditional Navier-Stokes equation subjected to the tangential velocity induced by the electroosmotic effect at the solid wall as a boundary condition, called the slip velocity (for example, the Helmholtz-Smoluchowski relation for the DC case). Despite such significant reduction in the computational effort, a reliable slip-velocity model to accurately describe the AC electroosmotic flow had not been proposed in literature until recently. Suh and Kang [19] showed that the electric layer near an electrode surface under an AC electric field should be of a triple-layer structure composed of the Stern layer, inner layer and middle layer (or buffer layer). Then, they presented a new asymptotic model for computing the slip velocity by incorporating the effect of the ion adsorption onto the electrode. The model consists mainly of solving the Laplace equation for the electric potential in the bulk region and a dynamic equation for the evolution of the surface charge on the electrode.

In the present study, we apply the theoretical model proposed by Suh and Kang [19] to the two-dimensional problem of AC electroosmosis on a pair of coplanar asymmetric electrodes embedded on the bottom wall of a rectangular channel to compute the slip-velocity distribution. To validate the model, we experimentally measure the slip velocity using micro-PIV technique and compare the experimental results with the numerical ones. Conclusions drawn through the present study can be briefly summarized as follows:

(i) For all the frequencies, the slip velocity has the highest values at the two inner edges of the pair of electrodes and then decreases exponentially to a zero value with going towards the two outer edges. The slip velocity on the narrow electrode is higher than that on the wide electrode. As the frequency increases, the slip velocity also increases, but the increase rate becomes lower.

(ii) To validate the theoretical model, the numerical slip-velocity profile ($\lambda_{Seff} = 40$nm and $\alpha = 0.8\times10^{-26}$) are compared with the experimental ones. Comparison results show that both profiles of the slip velocity on the wide electrode display an excellent agreement at all the frequencies considered in the present study. On the narrow electrode, on the other hand, they display different trends. Very good match between both profiles is seen at high frequencies (for example $\omega = 5{,}000$Hz), whereas very poor match is at low frequencies.

(iii) As the effective Stern-layer thickness (λ_{Seff}) increases, the slip velocity markedly decreases. It

is mainly because, with increasing layer thickness, the total potential drop across the Stern and inner layers increases and that across the inner layer decreases, finally leading to the reduction of the potential at the outer edge of the diffuse layer.

(iv) As the ion adsorption effect (denoted by α) increases, the slip velocity decreases. With increasing α, more counterions are absorbed at the interface between the Stern and inner layers, increasing the surface charge density. In such a case, there should be an increased jump in the potential gradient across the interface, finally decreasing the potential drop across the inner layer and thus the slip velocity.

Acknowledgment

This work has been supported by the Korea Science and Engineering Foundation (KOSEF) through the National Research Laboratory Program funded by the Ministry of Education, Science and Technology (No. 2005-1091).

References

[1] D. Li, *Electrokinetics in Microfluidics*, Elsevier, London, UK, (2004).

[2] N. G. Green, A. Ramos, A. González, H. Morgan and A Castellanos, Fluid flow induced by nonuniform ac electric fields in electrolytes on microelectrodes. III. Observation of streamlines and numerical simulation, *Physical Review E*, 66 (2002) 02635 (11 pages).

[3] S. Debesset, C. J. Hayden, C. Dalton, J. C. T. Eijkel and A. Manz, An AC electroosmotic micropump for circular chromatographic applications, *Lab Chip*, 4 (2004), 396-400.

[4] M. Z. Bazant and Y. Ben, Theoretical prediction of fast 3D AC electro-osmotic pumps, *Lab on a Chip*, 6 (2006), 1455-1461.

[5] N. Sasaki, T. Kitamori and H. B. Kim, AC electroosmotic micromixer for chemical processing in a microchannel, *Lab on a Chip*, 6 (2006), 550-554.

[6] S.-H. Huang, S.-K. Wang, H. S. Khoo and F.-G. Tseng, AC electroosmotic generated in-plane microvortices for stationary or continuous fluid mixing, *Sensors and Actuators B*, 125 (2007), 326-336.

[7] N. Loucaides, A. Ramos and G. E. Georghiou, Novel systems for configurable AC electroosmotic pumping, *Microfluidics and Nanofluidics*, 3 (2007), 709-714.

[8] J. P. Urbanski, J. A. Levitan, D. N. Burch, T. Thorsen and M. Z. Bazant, The effect of step height on the performance of three-dimensional ac electro-osmotic microfluidic pumps, *Journal of Colloid and Interface Science*, 309 (2007), 332-341.

[9] W. Hibler, B. Weiss, M. Mikolasek, R. Holly, K. Hingerl and B. Jakoby, Particle manipulation using 3-D ac electro-osmotic micropumps, *Journal of Micromechanics and Microengineering*, 18 (2008), 064016 (6 pages).

[10] H. S. Kwak and E. F. Hasselbrink Jr., Timescales for relaxation to Boltzmann equilibrium in nanopores, *Journal of Colloid and Interface Science*, 284 (2005), 753-758.

[11] H. M. Park, J. S. Lee and T. W. Kim, Comparison of the Nernst-Planck model and the Poisson-Boltzmann model for electroosmotic flows in microchannels, *Journal of Colloid and Interface Science*, 315 (2007), 731-739.

[12] S. Kang and Y. K. Suh, Numerical analysis on electroosmotic flows in a microchannel with rectangle-waved surface roughness using the Poisson-Nernst-Planck model, *Microfluidics and Nanofluidics*, DOI: 10.1007/s10404-008-0321-5 (2008).

[13] J.-B. Zhang, G.-W. He and F. Liu, Electro-osmotic flow and mixing in heterogeneous microchannels, *Physical Review E*, 73 (2006), 056305 (8 pages).

[14] T. J. Craven, J. M. Rees and W. B. Zimmerman, On slip velocity boundary conditions for electroosmotic flow near sharp corners, *Physics of Fluids*, 4 (2008), 043603 (14 pages).

[15] S. Dasgupta, A. A. S. Bhagat, M. Horner, I. Papautsky and R. K. Banerjee, Effects of applied electric field and microchannel wetted perimeter on electroosmotic velocity, *Microfluidics and Nanofluidics*, 5 (2008), 185-192.

[16] R. F. Probstein, *Physicochemical hydrodynamics: an introduction*, Wiley, New York, USA (2003).

[17] A. González, A. Ramos, N. G. Green, A. Castellanos and H. Morgan, Fluid flow induced by nonuniform ac electric fields in electrolytes on microelectrodes. II. A linear double-layer analysis, *Physical Review E*, 61 (2000), 4019-4028.

[18] M. R. Bown and C. D. Meinhart, AC electroosmotic flow in a DNA concentrator, *Microfluidics and Nanofluidics*, 2 (2006), 513-523.

[19] Y. K. Suh and S. Kang, Asymptotic analysis of ion transport in a nonlinear regime around polarized

electrodes under ac, *Physical Review E*, 77 (2008), 031504 (16 pages).

[20] H. S. Heo, S. Kang and Y. K. Suh, An experimental study on the AC electroosmotic flow around a pair of electrodes in a microchannel, *Journal of Mechanical Science and Technology*, 21 (2007), 2237-2243.

[21] A. Plecis and Y. Chen, Fabrication of microfluidic devices based on glass-PDMS-glass technology, *Microelectronic Engineering*, 84 (2007), 1265-1269.

[22] J. Santiago, S. Wereley, C. Meinhart, D. Beebe and R. Adrian, A particle image velocimetry system for microfluidics, *Experiments in Fluids*, 25 (1998), 316-319.

[23] S. Devasenathipathy, J. Santiago, S. Wereley, C. Meinhart and K. Takehara, Particle imaging techniques for microfabricated fluidic systems, *Experiments in Fluids*, 34 (2003), 504-514.

[24] J. S. Park, C. K. Choi and K. D. Kihm, Temperature measurement for a nanoparticle suspension by detecting the Brownian motion using optical serial sectioning microscopy (OSSM), *Measurement Science and Technology*, 16 (2005), 1418-1429.

Sangmo Kang received a B.S. and M.S. degrees from Seoul National University in 1985 and 1987, respectively, and then had worked for five years in Daewoo Heavy Industries as a field engineer. He also achieved a Ph.D. degree in the field of Mechanical Engineering from the University of Michigan in 1996. Dr. Kang is currently a Professor at the Division of Mechanical Engineering at Dong-A University in Busan, Korea. Dr. Kang's research interests are in the area of micro- and nanofluidics and turbulent flow combined with the computational fluid dynamics.